

I. INTRODUCTION

Due to its computational feasibility and relatively high accuracy, approximate Kohn-Sham density-functional theory (KS-DFT) simulations are the basis of present-day first-principles computational materials science ¹. Particle-particle interactions can require treatment beyond semilocal KS-DFT [1]. Experimental applications heavily rely on understanding and guiding electron-electron interaction. A relevant example of electron-electron interaction is scattering when an electron is scattered resulting in energy loss of the electron. Experimentally the electron loss spectrum can be realized by electron energy loss spectroscopy or inelastic scattering [2, 3].

Excited states can be accurately characterized by expensive Greens function techniques. By virtue of the Runge-Gross theorem [4] DFT can be extended to time-dependent processes. Time-dependent density-functional theory (TDDFT) is becoming an attractive alternative to many-body perturbation theory and can offer, in principle, an unbiased and independent framework complementary to experimental observations, enabling the interpretation of specific experimental observations and predictions of new materials with targeted properties.

Plasmon excitations are collective oscillations of electrons in the absence of an external electric field, that incorporate Coulomb interaction between electrons [5]. Due to the electron-electron interactions, plasmon excitations establish a high barrier when testing *ab initio* theories. When the external perturbation is weak, linear response TDDFT [6] is a useful tool to describe optical excitation energies. In TDDFT the electron loss or photoabsorption cross-section is quantified by the imaginary part of χ , the spatially nonlocal and dynamic density-density response function. The poles of the interacting density-density response function contain information about the optical excitation energies. The same density-density response function can deliver further information about the plasmons for a range of wavevectors.

Plasmon dispersion in nearly-free-electron alkali metals has attracted a great interest among experimentalists and theorists. The negative dispersion in the volume plasmon of the low-density alkali metals such as Rb and Cs has triggered a debate about the origin

density

goal here is to give an *a priori* numerical analysis why kernels by themselves (without the band-structure effects) can not predict negative dispersion in low density alkali metals. In this work we rely on the jellium model. The dimensionless parameters (r_s) for the jellium model corresponding to different metals are taken from Ref. [21]. We demonstrate that the exact constraints can lead to kernels that correctly predict a positive plasmon dispersion in jellium.

II. METHODOLOGY: EXCHANGE-CORRELATION KERNELS WITHIN LINEAR RESPONSE TDDFT

Nonempirical construction of density functionals has allowed widespread and successful applications of these approximations for the ground state [22]. Various exact constraints such as the uniform electron gas limit, Lieb-Oxford bound or the one-electron limit are known for the ground state [23]. According to linear response theory the interacting and noninteracting density-density response functions are coupled by the Dyson equation:

$$\chi_\lambda(q, \omega) = \chi_0(q, \omega) + \chi_0(q, \omega) (\lambda v_c(q) + f_{xc}^\lambda(q, \omega)) \chi_\lambda(q, \omega), \quad (1)$$

$\chi_\lambda(q, \omega)$ and $\chi_0(q, \omega)$ are the interacting and noninteracting response functions, respectively, $v_c(q) = \frac{4\pi\lambda}{q^2}$ and $f_{xc}^\lambda(q, \omega)$ are the Coulomb and exchange-correlation kernels. λ is the coupling constant that represents the adiabatic connection between a noninteracting Kohn-Sham ($\lambda = 0$) and the interacting real system ($\lambda = 1$) response. When Eq. 1 is applied to the uniform electron gas, $\chi_0(q, \omega)$ becomes the Lindhard function with complex frequencies [24], a basic component of our current research. In the adiabatic approximation, the exact kernel is a second functional derivative of the ground state exchange-correlation energy. In practice the exact kernel is unknown but can be modeled by satisfying exact physical constraints. Kernels are related to the “local field factors” as $G(q, \omega) = \frac{f_{xc}(q, \omega)}{-v_c(q)}$.

Many real systems have densities close to the paradigm uniform electron gas, as in alkali metals. The uniform electron gas is therefore a simple model system with physical relevance. All exchange-correlation kernels in this work model the uniform electron gas with known limiting behavior at $q \rightarrow 0$ and $q \rightarrow \infty$. The simplest approximation is known as the adiabatic local density approximation (ALDA) kernel for $\lambda = 1$ [25]:

$$f_{xc}^{ALDA}(q \rightarrow 0, \omega = 0) = -\frac{4\pi A}{k_F^2} \quad (2)$$

with $A = \frac{1}{4} - \frac{k_F^2}{4\pi} \frac{d^2(n\varepsilon_c)}{dn^2}$, where $k_F = (3\pi^2 n)^{1/3}$ is the Fermi wavevector and ε_c the correlation energy per particle of the uniform electron gas. $A = \frac{1}{4}$ belongs only to the exchange-only ALDA, while the density-dependent term in A gives the correlation beyond the high-density limit.

The real-space representation of ALDA is a delta function which indicates the spatial locality of this kernel. ALDA gives reasonable accuracy for low-frequency, long-wavelength excitations, but is not the right choice for a general correction to RPA [25]. The ALDA kernel was applied to the ground state correlation energy of the uniform electron gas but makes an error of ~ 0.5 eV [26]. This error is the same in magnitude but of opposite sign to the error that RPA makes for the same system.

The ALDA kernel can be made nonlocal, by applying a cutoff that makes the exchange-correlation kernel cancel the Hartree kernel for $q > 2k_{cut}$. The cutoff is introduced by the renormalized ALDA (rALDA) expression [27]

$$f_{xc}^{rALDA}(n, q) = -[\theta(k_{cut} - q) \frac{4\pi}{k_{cut}^2} + \theta(q - k_{cut}) \frac{4\pi}{q^2}] \quad (3)$$

where k_{cut} is the cutoff wavevector. The rALDA kernel has the same form as the ALDA kernel with the cutoff wavevector $k_{cut} = \frac{k_F}{\sqrt{A}}$. By construction the rALDA_{xc} kernel keeps the correct $q \rightarrow 0$ limit of ALDA, but improves the wrong $q \rightarrow \infty$ behavior of ALDA_{xc}. For inhomogeneous systems, more ingredients like the density gradient or the kinetic energy density give more flexibility for kernels, as for ground state density functional approximations. The kinetic energy density is one of the ingredients of the nonlocal energy optimized (NEO) exchange-only kernel [28].

The NEO kernel improves the ground state correlation energy and structural properties of real systems beyond RPA [28]. The NEO kernel is designed to satisfy further physical constraints beyond both ALDA or rALDA, and has the form

$$f_x^{NEO} = -\frac{4\pi}{2q^2} [1 - e^{-\beta q^2/k_F^2}] \quad \text{reached when } \checkmark \quad \text{equals } 1 \quad (4)$$

where $\beta = \frac{1}{4\tilde{c}(1-z^2)}$. The one-electron limit is satisfied by the ingredient $z = \frac{\tau^w}{\tau}$, where τ^w is the one-electron kinetic energy density [29] and τ the positive kinetic energy density constructed from the Kohn-Sham orbitals. In the uniform electron gas, z is zero. When $q \rightarrow 0$, the NEO kernel is properly independent of q for the uniform electron gas. The parameter \tilde{c} has a key relevance to the current work. In the construction of NEO, \tilde{c} is designed to give a correction to the RPA correlation energy in the high-density limit. In other words, the standard $\tilde{c} = 0.264$ parameter in NEO provides a unique fit to the exact second-order correlation energy for the spin-unpolarized electron gas. The “second-order exchange” contribution to the second-order correlation energy of the uniform gas is the correction to direct RPA from wavefunction anti-symmetry that survives in the high-density limit. It can be evaluated from explicit expressions given by von Barth and Hedin for RPA [30] and by Langreth and Perdew [18] beyond RPA.

β can be chosen to satisfy another constraint relevant to the long-wavelength ($q \rightarrow 0$) limit. This choice is also made in the ALDA, rALDA, and in the CP07 dynamic exchange-correlation kernel constructed by Constantin and Pitarke [31]. The compressibility sum rule, [32] as

$$f_{xc}(n; q \rightarrow 0, \omega = 0) = \frac{d^2}{dn^2} [n\varepsilon_{xc}(n)], \quad (5)$$

is an important requirement for frequency-dependent exchange-correlation kernels. Satisfying the compressibility sum rule β becomes

$$\beta = \frac{4\pi}{2k_F^2 4\tilde{c}} = -\frac{2k_F^2}{4\pi} \frac{d^2}{dn^2} [n\varepsilon_{xc}(n)] = \frac{2}{A} \quad (6)$$

or $\tilde{c} = 0.5$ in the high-density limit.

Thus the energy optimization of $\tilde{c} = 0.264$ in the high-density limit is different from the value $\tilde{c} = 0.5$ that yields the correct small- q kernel in the high-density limit. In the next section we will extensively discuss the impact of these physical constraints on the plasmon dispersion and provide a novel insight about the role of correlation effects. It will turn out that the difference between the ALDA and NEO kernels is important for the correlation

resolution electron energy loss (EELS) experiments indicate that the plasmon dispersion in heavy alkali metals such as Rb and Cs becomes negative, i.e., the plasmon frequency decreases with increasing wavevector q [7]. Since all the above experiments and calculations were performed for periodic crystals, it is difficult to decouple correlation and band structure effects [33] in the decay of the plasmon excitations.

Further calculations by Ku and Eguiluz in K crystal [10] indicate the relevance of band structure versus correlation and demonstrate that the exchange-correlation effects beyond RPA at the ALDA level have only a minor role in the decay of plasmons. A similar observation was made by Quong and Eguiluz [34] for Na crystal. Although crystal periodicity is important when modeling realistic conditions, the jellium model can offer an important way to separate the impact of many-body correlations and band structure. Within our work we want to provide an additional theoretical and numerical insight only about the many-body correlation effects and explain why in general no beyond-RPA approximation for jellium can predict the correct plasmon dispersion and lifetime for Cs. The justification of our results is based merely on exact physical constraints imposed on the construction of beyond-RPA approximations. By using the jellium model for alkali metals, we can build upon the conclusion that ALDA gives a minor improvement beyond RPA for the plasmon dispersion. With the possession of nonlocal exchange-correlation kernels developed since the later 90's, we can make further conclusions about how these recent approximations compare to ALDA and RPA in terms of correlation effects.

We can make two groups of assessed approximations. The first group includes exchange-only and exchange-correlation kernels based on the ALDA approximations. ALDAx and ALDAxc are both local kernels but differ in correlation contribution. rALDAx and rALDAxc are nonlocal. The second group consists of NEO exchange-only kernels [28] with the \tilde{c} parameter constructed by satisfying different physical constraints. The default version of the NEO kernel yields the exact correction to the RPA correlation energy of jellium in the high-density limit:

$$e_c^{2x} = \frac{3}{8\pi^3} \int_0^\infty dQ Q^2 \tilde{G}_x(Q) \int_0^\infty dW Q^2 \{2\beta(Q, W)\}^2, \quad (7)$$

[19]

where $\tilde{G}_x(Q)$ refers to the kernel, according to the correspondence between kernels and local-field factors. $Q = \frac{q}{2k_F}$ is a dimensionless wavevector, and $W = \frac{\Omega}{2k_F^2}$ is a dimensionless frequency, to obtain the explicit expression for the second-order exchange energy e_c^{2X} by Langreth and Perdew [18] beyond RPA using the RPA correlation energy for the uniform electron gas given by von Barth and Hedin. The \tilde{c} parameter that corresponds to the second-order correlation energy was found to be 0.264.

Alternatively, in the long-wavelength limit we can use the compressibility sum rule formulated as $\frac{d^2}{dn^2} [n\epsilon_{xc}(n)]$ to determine “ \tilde{c} ”. Then the \tilde{c} parameter of NEO can be estimated from the compressibility sum rule of the ALDAxc expression. This fitting delivers a different $\tilde{c} = 0.43 - 0.47$ at metallic densities considered here. While formally the NEO approximation remains an exchange-only kernel, this kind of fitting to an exact physical condition with an exchange-correlation approach brings the correlation effects relevant for metallic densities into our NEO kernel [31].

long-wavelength effects

Clearly “ \tilde{c} ” controls the correlation or screening within the NEO approximation starting from $\tilde{c} \rightarrow \infty$ in RPA. The impact of “ \tilde{c} ” as a screening parameter on ground state correlation energies was established by Bates et al in 2016. Changing “ \tilde{c} ” from its default 0.264 value was shown to yield different correlation energies in the uniform electron gas at $r_s=4$.

The exchange-only NEO kernel can be explicitly turned into an exchange-correlation approach by replacing “ \tilde{c} ” by an electron-density-dependent parameter. This approach was tested for jellium slab correlation energies at moderate densities, and resulted in improved integrated correlation energy [35]. For a given density, the density dependence can make “ \tilde{c} ” significantly smaller than its default value. In our analysis we investigate the effect of a low “ \tilde{c} ” parameter on the plasmon dispersion of various NFE metals. For testing purposes we choose $\tilde{c} = 0.0037$. Notice that this choice of \tilde{c} represents an unphysically low density according to Eq. (13) of Ref. 35.

At first we discuss the plasmon dispersion up to the wavevector region where plasmons decay into single particle excitations. We consider all the exchange-correlation kernels described above. Within the static approximation for the kernel $f_{xc}(q)$, the plasmon frequency

$\omega_p(q)$ is found by solving the equation $\epsilon(q, \omega) = 1 - (v_c(q) + f_{xc}(q)) \chi_0(q, \omega) = 0$, for $\lambda = 1$,¹⁷ and the solutions are undamped outside the particle-hole continuum, i.e., for $q < q_c$ where $\frac{\omega_p(q_c)}{\varepsilon_F} = 2 \left(\frac{q_c}{k_F} \right) + \left(\frac{q_c}{k_F} \right)^2$. For the r_s values considered here, $q_c/k_F \approx 1 \ll k_{cut}/k_F \approx 2$, where k_{cut} is the cutoff wavevector for a kernel. Thus rALDA and ALDA kernels will yield the same plasmon dispersion.

Al is a metal with rather high density, and RPA becomes relatively exact in the high-density limit [34]. Here, we model Al by jellium with $r_s = 2.07$. The small wavevector behavior is demonstrated by the correct plasmon energy known from an EELS experiment [36]. All ALDA and rALDA kernels return the correct long-wavelength limit of RPA. The $\tilde{c} = 0.47$ NEO exchange kernel keeps the correct long-wavelength of RPA. Since the compressibility sum rule delivers direct information about the long-wavelength limit, among all the approximations NEO $\tilde{c} = 0.47$ has a direct impact on the curvature of the dispersion. The fitting against this exact constraint designates that the plasmon dispersion must start out as horizontal at small wavevectors. NEO $\tilde{c} = 0.47$ exemplifies the best behavior in the long wavelength limit ($q \rightarrow 0$) that any static kernel for jellium at $r_s = 2.07$ can demonstrate.

Comparing the ALDA and rALDA kernels in the left panel of Fig. 2, it is apparent that the nonlocal feature of the rALDA is much relevant in the ground state correlation energy does not change the plasmon dispersion, and all ALDA and rALDA approximations yield the same dispersion curve. The NEO $\tilde{c} = 0.264$ and $\tilde{c} = 0.47$ methods basically agree, while the NEO $\tilde{c} = 0.0037$ is completely unphysical with low plasmon frequencies as an indication of the lack of exact constraints (See Fig. 2).

For jellium at $r_s=3.93$ (as for Na), all ALDA and rALDA dispersion curves barely differ in the left panel of Fig. 3. As in Al, there is no significant change coming from the nonlocal kernels. According to the right subfigure, the NEO $\tilde{c} = 0.264$ and NEO $\tilde{c} = 0.44$ kernels differ more than they do in Al for a range of ~ 0.5 for dimensionless wavevector Q. NEO $\tilde{c} = 0.0037$ leads to unphysically low plasmon frequencies.

Cs is the alkali metal with the lowest density [37]. We modeled it here as jellium with $r_s = 5.62$. This characteristic manifests itself in the plasmon dispersion when comparing the approximations in the left and right panels of Fig. 4. Being correct at small q , the

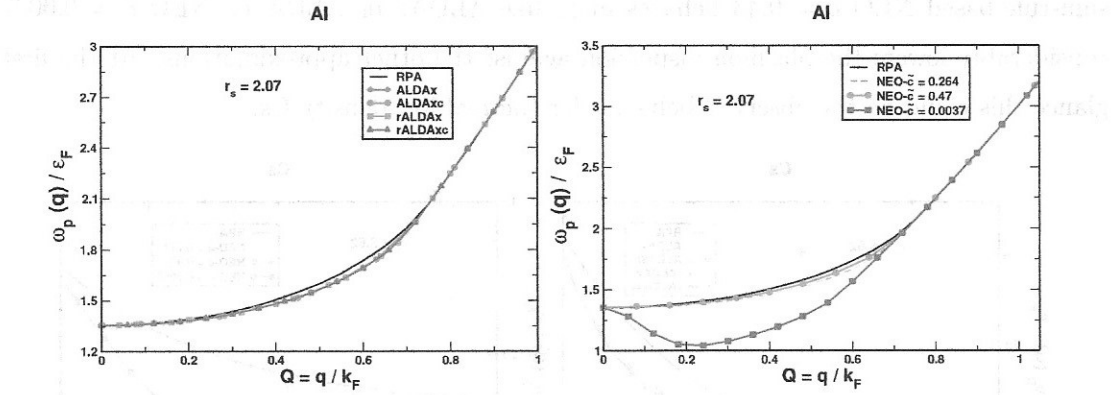


FIG. 2. The plasmon dispersion for Al (modeled with jellium with $r_s = 2.07$) up to the critical wavevector. The left panel shows the dispersion obtained with RPA and beyond-RPA with ALDAx, ALDAxc, rALDAx and rALDAxc approximations. The right panel shows the dispersion from RPA and the three NEO approximations with the \tilde{c} parameters corresponding to different choices.

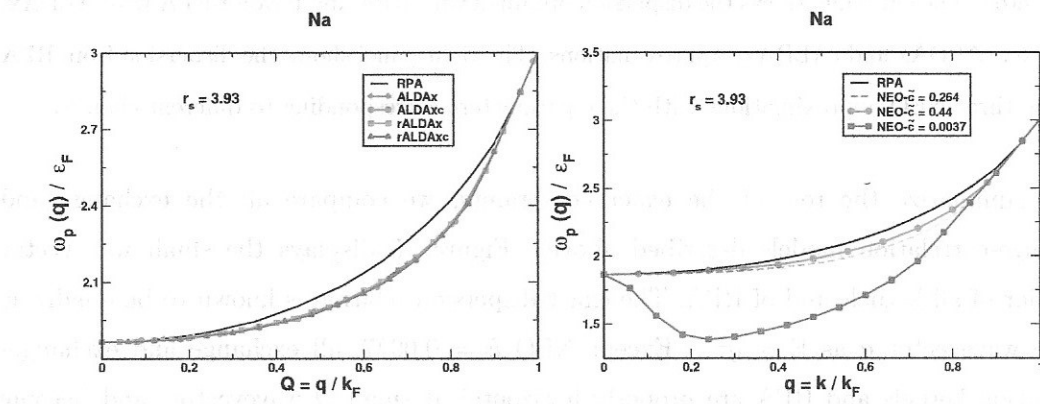


FIG. 3. The plasmon dispersion for Na (modeled with jellium with $r_s = 3.93$), up to the critical wavevector. The left panel shows the dispersion obtained with RPA and beyond-RPA with ALDAx, ALDAxc, rALDAx and rALDAxc approximations. The right panel shows the dispersion from RPA and the three NEO approximations with the \tilde{c} parameters corresponding to different choices.

than ALDAX

ALDAxc and rALDAxc are more suitable for lower densities in Cs, however, the nonlocality versus locality in rALDAxc and ALDAxc does not much affect the dispersion. Comparing the NEO approximations, NEO $\tilde{c} = 0.264$ results in more correction beyond-RPA than it does in the previous two metals. Furthermore NEO $\tilde{c} = 0.264$ yields more correction in the plasmon frequencies than any of the ALDA and rALDA kernels. The exact compressibility-

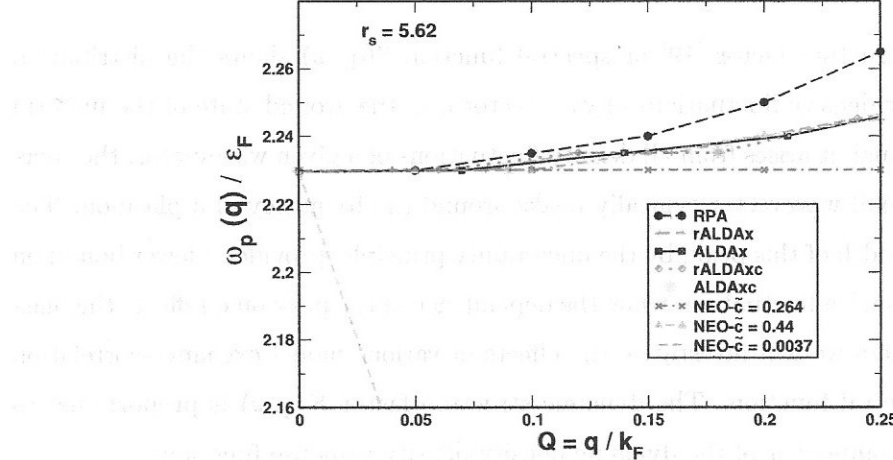


FIG. 5. The long wavelength behavior or all approximations considered in this work.

band structure sample the Brillouin zone. Our calculations including bandstructure effects confirm that the band structure significantly alters the plasmon dispersion for Cs, while its effect is negligible for Na. The plasmon frequency at $q \rightarrow 0$ shows a 0.5 eV renormalization compared to the RPA value within the jellium model. The effect of the band structure in Cs is significantly large enough to dominate over the changes from one kernel to another.

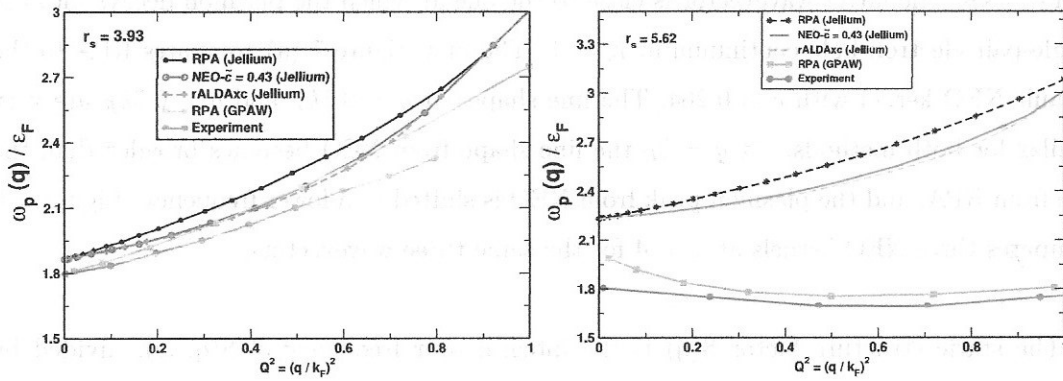


FIG. 6. The plasmon dispersion of Na (left) and Cs (right) with RPA and some exchange-correlation kernels within the jellium model. For Cs, the dispersion with RPA is also displayed with band-structure effects obtained from the GPAW code, showing results close to experiment [7] (also shown).

structure factor found by integrating $S_\lambda(q, \omega)$ over frequency and dividing by the electron number. According to the expression given by Eq. 9, the exchange-correlation energy depends upon the dynamic structure factor. The exchange energy E_x replaces S_λ by S_0 , and the correlation energy is $E_c = E_{xc} - E_x$. Figure 8 shows the wavevector decomposition of the correlation energy for all exchange and exchange-correlation kernels considered here. We plot this for $r_s = 4$ and $r_s = 5.62$.

The physical basis of our analysis is the exact exchange-correlation kernel $f_{xc}(q, \omega)$ of the uniform electron gas. For the correlation energy, the static version of the kernel $f_{xc}(q, 0)$ can be applied to a good approximation [26]. Note that the frequency dependence at least qualitatively can also be ignored for $\omega \approx \omega_p$ [45, 46]. The ALDA exchange-correlation kernel $f_{xc}^{ALDA}(q, 0)$ approaches the exact kernel for the uniform electron gas at $q \rightarrow 0$. In the long wavelength limit,

$$\lim_{q \rightarrow 0} f_{xc}(q, 0) = \lim_{q \rightarrow 0} f_{xc}^{ALDA}(q, 0). \quad (10)$$

As we will see below, f_{xc}^{ALDA} breaks down for $q/2k_F \geq 0.5$, where our constraint-based NEO kernels become less negative and more accurate. Therefore, as suggested by Fig. 1:

$$f_{xc}^{ALDA}(q, 0) < f_{xc}(q, 0) < 0 \quad (11)$$

The ALDA approximation becomes a lower bound to the static exact exchange-correlation kernel for the correlation energy of the uniform electron gas. Figure 8 visualizes the relation between ALDAxc, RPA and some other exchange-correlation kernels. The ALDAxc is shown in the left panel of Figure 8. The ALDAc is very accurate for small wavevectors but starts to deviate from RPA at $Q \approx 0.25$. At $q = 2k_F$ the ALDAxc yields a strong overestimation of the correction to RPA correlation energy. All static beyond-RPA kernels make the exchange-correlation energy of RPA less negative for any density including $r_s = 5.62$. The correlation energies from NEO $\tilde{c} = 0.264$ and from the NEO kernel fitted against the compressibility sum-rule are close to each other but the unphysical NEO $\tilde{c} = 0.0037$ adds a much larger correction to the RPA correlation energy.

The constraints of Equations 10 and 11 control the plasmon dispersion and the correlation

energy. The dynamic structure factor becomes a link that couples the physics in the correlation energy and plasmon dispersion. From the correlation energy, the exact uniform-electron gas-based kernel must be less negative than the ALDA_{xc} kernel. The NEO $\tilde{c} = 0.264$ kernel is uniform electron gas-based only through its energy optimization to the high-density limit, and performs reasonably for both plasmon dispersion and correlation energy in jellium.

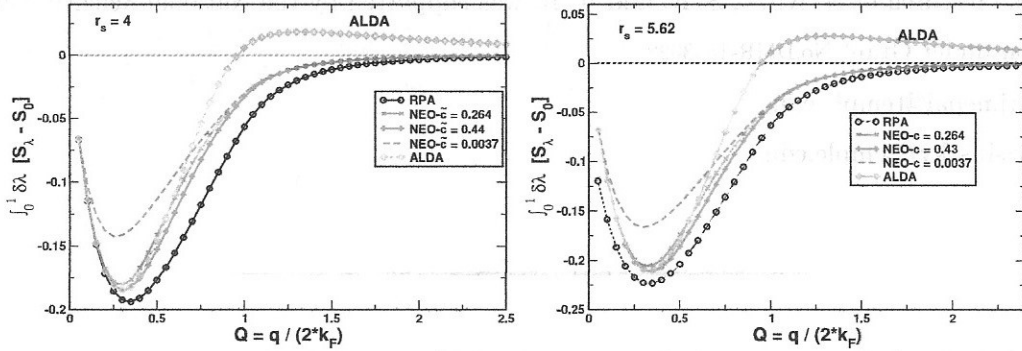


FIG. 8. Wavevector analysis of the ground state correlation-only energy of jellium from the dynamic structure factor for reduced wavevector $Q = \frac{q}{2k_F}$. The area under the curve is the correlation energy. The left figure shows the correlation-only energy for RPA, ALDA and NEO with the three choices for \tilde{c} , for $r_s=4$. The right figure shows the same for $r_s=5.62$ corresponding to Cs.

V. CONCLUSION

We have presented various model exchange-correlation kernels beyond-RPA for the plasmon dispersion within the jellium model for alkali metals. We have shown that the plasmon dispersion is strictly controlled by exact constraints. Additional physics beyond the ALDA kernel, such as nonlocality in space, can be unimportant for plasmon excitations. In change, physical constraints such as the compressibility sum rule determine the plasmon decay with exchange-correlation kernels. Clearly none of our methods based on particle-hole RPA for jellium is able to predict the experimentally observed negative plasmon dispersion for the heavy alkali metal Cs which arises from bandstructure. The current exchange-correlation kernels do not have an explicit density dependence that could have a larger impact. For the exact exchange-correlation kernel, the ALDA_{xc} is likely a lower bound (as suggested by Fig. 1). The ALDA_{xc} is accurate for $\frac{q}{k_F} < 1$, the range of q that determines the plasmon

dispersion, even though the ALDAxc kernel fails badly for $\frac{q}{k_F} \gg 1$, a range that contributes significantly to the correlation energy.

VI. ACKNOWLEDGMENT

The research of N. K. N., S. R. and A. R. was supported by the National Science Foundation under Grant No.DMR-1553022. *We thank John P. Perdew for comments on the manuscript.*

* niraj.nepal@temple.edu

† aruzsinszky@temple.edu

-
- [1] G. Onida, L. Reining, and A. Rubio, Rev. Mod. Phys. **74**, 601 (2002).
 - [2] H. Raether, *Excitation of plasmons and interband transitions by electrons*, Vol. 88 (Springer, 2006).
 - [3] W. Schülke, J. Schmitz, H. Schulte-Schrepping, and A. Kaprolat, Phys. Rev. B **52**, 11721 (1995).
 - [4] E. Runge and E. K. Gross, Phys. Rev. Lett. **52**, 997 (1984).
 - [5] D. Pines, *Elementary Excitations in Solids* (Benjamin, New York, 1964).
 - [6] M. Petersilka, U. Gossman, and E. Gross, Phys. Rev. Lett. **76**, 1212 (1996).
 - [7] A. Vom Felde, J. Sprösser-Prou, and J. Fink, Phys. Rev. B **40**, 10181 (1989).
 - [8] D. Pines and P. Nozières, *The Theory of Quantum Liquids V. 1: Normal Fermi Liquids* (Benjamin, 1966).
 - [9] F. Aryasetiawan and K. Karlsson, Phys. Rev. Lett. **73**, 1679 (1994).
 - [10] W. Ku and A. G. Eguiluz, Phys. Rev. Lett. **82**, 2350 (1999).
 - [11] M. Taut, J. Phys. Condens. Matter **4**, 9595 (1992).
 - [12] M. Taut and K. Sturm, Solid State Commun. **82**, 295 (1992).
 - [13] D. Bohm and D. Pines, Phys. Rev. **92**, 609 (1953).
 - [14] N. K. Nepal, A. Ruzsinszky, and J. E. Bates, Phys. Rev. B **97**, 115140 (2018).
 - [15] N. K. Nepal, S. Adhikari, J. E. Bates, and A. Ruzsinszky, Phys. Rev. B **100**, 045135 (2019).
 - [16] L. Schimka, R. Gaudoin, J. c. v. Klimeš, M. Marsman, and G. Kresse, Phys. Rev. B **87**,